

Segmentation of the Left Ventricle of the Heart in 3-D+t MRI Data Using an Optimized Nonrigid Temporal Model

Michael Lynch*, Ovidiu Ghita, and Paul F. Whelan, *Senior Member, IEEE*

Abstract—Modern medical imaging modalities provide large amounts of information in both the spatial and temporal domains and the incorporation of this information in a coherent algorithmic framework is a significant challenge. In this paper, we present a novel and intuitive approach to combine 3-D spatial and temporal (3-D + time) magnetic resonance imaging (MRI) data in an integrated segmentation algorithm to extract the myocardium of the left ventricle. A novel level-set segmentation process is developed that simultaneously delineates and tracks the boundaries of the left ventricle muscle. By encoding prior knowledge about cardiac temporal evolution in a parametric framework, an expectation-maximization algorithm optimally tracks the myocardial deformation over the cardiac cycle. The expectation step deforms the level-set function while the maximization step updates the prior temporal model parameters to perform the segmentation in a nonrigid sense.

Index Terms—Cardiac magnetic resonance imaging (MRI), four-dimensional (4-D), level-set, segmentation, temporal model.

I. INTRODUCTION

RECENT studies indicate [1] that cardiovascular disease (CVD) claims more lives each year than the next five leading causes of death combined. The World Health Organization's 2002 report [1], states that 29.3% of deaths in 191 countries were as a result of CVDs. The British Heart Foundation [2] shows that CVDs account for 42% of deaths in the European Union. Quantitative measurement of the left ventricle of the heart is used as a key indicator of cardiac health. Analysis of the heart function is achieved through the segmentation of the left ventricle. From this accurate segmentation, prognostic measurements used in the diagnosis of CVDs can be obtained. These features include the ejection fraction (EF) of the left ventricle cavity, the left ventricle mass (LVM) of the myocardium, wall thickness and wall thickening (WT) of the left ventricle myocardium. For a full definition of the classical features used in the evaluation of cardiac health, see Frangi *et al.* [3].

Cardiac data is increasingly available in 3-D + time, therefore, it is believed that the best approach is to apply an appro-

priate technique to the entire dataset presented from a patient scan. Many researchers have attempted to address the segmentation problem in 3-D + time data. Often, temporal coherence in the data is incorporated using sequential approaches, where a robust initial segmentation (this is often manually assisted) forms the initialisation for subsequent volumes throughout the cardiac cycle.

There are a number of challenges in segmenting the myocardial muscle in 4-D (3-D+time) cardiac magnetic resonance imaging (MRI) data. First, the inherent noise associated with cine MRI that is caused by factors such as the patient movement, cardiac dynamics, partial voluming effects, and coil intensity fall off is an important issue that must be addressed. Second, the vast amount of data presented from a single cardiac study makes the manual landmarking of features required by supervised algorithms impractical. Finally, it is preferred to find appropriate methods to incorporate information of the cardiac dynamics into the image segmentation. Therefore, it is the aim of this paper to develop a methodology that fuses the local image information while incorporating a global temporal model that reflects the physical dynamics of the cardiac muscle during the cardiac cycle. The proposed algorithm performs a contour evolution that incorporates image data and temporal data in an intuitive manner.

Many boundary based segmentation methods such as active contours (snakes) [5] have been developed for use in medical image object extraction. Generally, the aim of boundary based segmentation methods is to deform a closed curve using both the intrinsic properties of the curve and image information to capture the target object [4]. This form of segmentation has some advantages over statistical intensity based partitioning algorithms as object shape is one of the key factors in the evolution of the contours. There are a large number of applications in medical image analysis where anatomical features can be encapsulated within a closed contour. From their introduction, snakes have received a large amount of interest from the vision community and significant research has been performed in extending the original snake formulation. Such extensions include controlling the snake's propagation and this can be achieved by using parametrically deformable models [6], [7], deformable triangulated meshes [8]–[11], and Gaussian distributed *a priori* models that were incorporated in the development of the active shape and active appearance models [12]–[16]. Lorenzo-Valdés *et al.* [17] construct a probabilistic atlas of manually segmented temporally aligned data. Automatic segmentation is achieved by registering the atlas on the data and using this as the initial values

*M. Lynch is with Siemens AG, 91058 Erlangen, Germany. (e-mail: lynchm@eeng.dcu.ie)

O. Ghita and P. F. Whelan are with Vision Systems Group, Dublin City University, Dublin 9, Ireland.

Color versions of one or more of the figures in this paper are available online at <http://ieeexplore.ieee.org>.

Digital Object Identifier 10.1109/TMI.2007.904681

for an expectation maximization (EM) algorithm. The EM algorithm is then iterated until convergence and this is followed by the application of a final classification step where the Markov random fields (MRF) and largest connected components (LCC) are employed to refine the initial segmentation.

This paper describes a novel method for the segmentation of 4-D cardiac MRI data using *a priori* knowledge about the temporal deformation of the myocardium that is embedded in a level-set scheme. By exploiting the Eulerian formulation of the level-set, the extension to a complete 4-D segmentation is achieved by calculating a parametric model of the left ventricle deformation over a cardiac cycle. This model is then iteratively refined using an optimization algorithm. Therefore, our approach infers a loose model to the temporal motion for the continuous temporal evolution of the boundary surfaces. The initial temporal model is iteratively updated to better fit the data in a novel way which can correct initialization errors, increase the convergence speed, and provide temporal smoothing. This paper introduces the level-set theory, followed by a description of two approaches that incorporate the temporal motion of the heart in the level-set evolution. We show that an approach based on updating the temporal model using an EM algorithm proved to be the optimal solution to segment the left ventricle cavity in the cardiac 4-D data. The proposed method is then extended by coupling two level-sets to segment and track the inner and outer walls of the left ventricle myocardium and experimental results are given.

II. LEVEL-SET METHOD

Level-sets were first introduced by Osher and Sethian [18] which extended the snake formulation to an Eulerian formalisation. Malladi *et al.* [19], [20] and Caselles *et al.* [21], [22] showed how level-set algorithms could be applied for enhancement and shape recovery in medical images using edge-based stopping terms. An extension of Malladi's work performed by Niessen *et al.* [23] used a more diffusive propagation term to increase the influence of the stopping term. An extensive review of level-set methods is given by Suri *et al.* [24] and also by Angelini *et al.* [25]. Boundary based level-set formulation can also be thought of as transforming the earlier work of Kass *et al.* [5] on active contours from a Lagrangian to an Eulerian formulation. Like active contours, the deformation of the level-set is seen as a gradient flow to a state of minimal energy, providing the object to be segmented has clearly identifiable boundaries [19]–[22], [26].

The basic property of the level-set can be described as extending the dimensionality of the solution to $N + 1$, where N is the initial dimension of the problem. Consequently, some advantageous properties can be exploited. The evolving curve, or front Γ , evolves as the zero level-set of a higher dimensional function ϕ where $\phi_\tau = \partial\phi/\partial\tau$ and τ represents the iteration of the level-set

$$\begin{aligned} \phi_\tau + F|\nabla\phi| &= 0 \\ \phi(s, \tau = 0) &= \text{given.} \end{aligned} \quad (1)$$

This function deforms with a force F that is dependent on both curvature of the front and external forces in the image.

The force acts in the direction of the normal to the front. The term “given” refers to an initial boundary surface from which ϕ evolves. s defines a position in space as (x, y, z) coordinates.

The use of level-sets for segmentation of the cardiac muscle in MRI is appropriate for the following reasons.

- One can perform numerical computations involving curves and surfaces on a fixed Cartesian grid without having to parametrize these objects (Eulerian, nonmarker based solution).
- It becomes easier to implicitly track shapes which undergo topological changes such as situations when a shape splits in two, develops holes, or the reverse of these operations (although this scenario is not present when working in volume data).
- Intrinsic geometric properties of the front, such as the curvature and normals, can be easily calculated.
- The method can be extended to higher dimensions.

The fundamental objective behind level-sets is to track a closed interface $\Gamma(\tau)$, for which $\Gamma(\tau) : [0, \infty) \rightarrow \underline{R}^N$, as it evolves in the data space. The interface is represented by a curve in 2-D and a surface in 3-D, which are the set of points that are on the boundaries of the region of interest Ω . The theory behind level-set segmentation is largely based on work in partial differential equations and the propagation of fronts under intrinsic properties such as curvature [18], [27]. Level-set theory aims to exchange the Lagrangian formalization and replace it with an Eulerian form, where the initial valued partial differential equations control the front (boundary) evolution. Representing the boundary as the zero level-set instance of a higher dimensional function ϕ , the effects of curvature can be easily incorporated. ϕ is represented by the continuous Lipschitz function $\phi(s, \tau = 0) = \pm d$, where d is the signed distance from position s to the initial interface $\Gamma(0)$ [see (2)]. The distance is given a positive sign outside the initial boundary ($R^n \setminus \Omega$), a negative sign inside the boundary ($\Omega \setminus \partial\Omega$) and zero on the boundary ($\partial\Omega$)

$$\phi(s) = \begin{cases} -d & \forall s \in \Omega \setminus \partial\Omega \\ 0 & \forall s \in \partial\Omega \\ +d & \forall s \in R^n \setminus \Omega \end{cases}. \quad (2)$$

From this definition of ϕ , intrinsic properties of the front can be easily determined, i.e., the normal $\vec{n} = \pm\nabla\phi/|\nabla\phi|$ and the curvature $\kappa = \nabla\nabla\phi/|\nabla\phi|$.

Also by analysing (2) in more detail, ϕ can be considered as a function in two different ways. First, ϕ can be considered as a static function $\phi(s)$ that is evaluated at particular instances or isovalues. This leads to the formulation of the Eikonal equations and is discussed in more detail in Section II-A. Alternatively, ϕ can be described as a dynamic function $\phi(s, t)$ that evolves through time and the closed contour, or front, is the special case where the value of $\phi(s, \tau)$ equals zero. Using this definition, it can also be said that at any time t_0 , the set of points that define a curve can be represented as the function $\phi(s, \tau_0) = 0$. It is also clear that as the curve evolves through time, the function ϕ also evolves. Consider a point $s(\tau)$ on the contour that is evolving through time, i.e., $\phi(s(\tau), \tau) = 0$. By the chain rule

$$\phi_\tau + s'(\tau)\nabla\phi = 0. \quad (3)$$

The force is defined as $F = s(\tau)\vec{n}$ and can be interpreted as a force that moves the point $s(\tau)$ in the normal direction \vec{n} . If \vec{n} is replaced with $\vec{n} = \pm \nabla\phi/|\nabla\phi|$, the equation takes the form of a Hamilton-Jacobi as expressed in (1). If the force term is rewritten as $F = F_0 + \epsilon\kappa$ to include a constant advection term F_0 , analogous to the inflation force used in some deformable models, the evolution of ϕ becomes

$$\phi_\tau = -F_0|\nabla\phi| + \epsilon\kappa|\nabla\phi| \quad (4)$$

where the parameter ϵ is a user defined curvature term.

To speed up the implementation, the update is only performed within a narrowband [28] surrounding the boundary interface, which is defined within a constant distance from the front. In our case, the narrowband was determined experimentally to six voxels and it is redefined every three iterations. The parameters ϵ and β [see (8)] were also determined experimentally and represent the influence of the curvature and attraction to the gradient on the evolving boundary, respectively. The mean curvature is calculated directly from the function ϕ .

A. Initialization Using Fast Marching

In order to overcome the ‘‘myopic’’ characteristics of level-set propagation, Sethian [27] introduced a Fast Marching method. This is the unique case of the level-set where the force F is always greater than zero and this propagates a monotonically advancing front. If the 2-D case is considered again, a set $T(s)$ is created that defines the time at which the front Γ crosses the position s . T satisfies the equation

$$|\nabla T|F = 0. \quad (5)$$

The evolution is iteratively assessed by solving the roots of the quadratic equation of the Eikonal equation and sorting the values of T with respect to size. The stopping term is based on the diffusion of the gradient and can be calculated as

$$F_s = e^{-\alpha|\nabla I_s|} \quad (6)$$

where α is a user defined term and $|\nabla I_s|$ is the absolute value of the gradient. The Fast Marching approach gives an approximate segmentation and is used for the evaluation of the initial contour for the dynamic level-set method. The results from the Fast Marching algorithm can be seen in Fig. 2.

III. APPLICATION TO 4-D DATA

Fritscher *et al.* [29] aimed to apply full 4-D information to boundary driven and region-competition geodesic contours. In this initial work, principal components analysis (PCA) was performed on signed distance maps to create models, where the mean of these models were used to initialize the level-set algorithm. In the 4-D segmentation work described in Bardinet *et al.* [30] and also in McInerney *et al.* [31], the temporal dimension was considered in a sequential approach where the segmentation from the previous time frame was used as the initialization for the current time frame. Rueckert and Burger [32] also used this sequential approach where the shape at time $(t + 1)$ was a deformation of the shape at time frame t . The deformation is achieved using energy minimization of the deformable template in a Bayesian

formulation. Sun *et al.* [33] created a nonlinear dynamic model learned from a set of training data. A manual tracing of the first image in the sequence is used to create a posterior density estimate of the left ventricle at each time frame. A curve evolution is then performed with the maximum posterior estimate. McEachen and Duncan [34] performed tracking of the left ventricle by performing point correspondence from time t to $t + 1$ in which they assumed a small degree of motion between time frames. Based on these assumptions, a smooth transition of the parametric contours is achieved using an optimization algorithm.

Paragios [35] introduced an energy constraint into his variational level-set approach that enforced a intensity consistency throughout the temporal cycle. A transformation is calculated between time I_t and I_{t+1} based on a bounded error function, where I_t represents the intensity value at time t . In Montagnat and Delinette [36], the deformable model is influenced by introducing time-dependent constraints. These consist of prior temporal knowledge through either temporal smoothing or trajectory constraints. Perperidis *et al.* [37], [38] used a spatial temporal model found by experimentation to perform spatio-temporal registration of cardiac MR images.

Segmentation in 3-D+time should perform a segmentation of the 3-D volumes and use this information in the time domain. To this end, a number of approaches are proposed with the advantages and disadvantages of each discussed.

- **Sequential Approach** consists of naively using the results from time sequence t as the initialization for time sequence $t + 1$. This approach assumes no prior knowledge about the temporal dynamics of the heart. The only assumption is that the cardiac muscle boundaries do not exhibit large movements between time sequences. In this approach, errors are propagated throughout the cycle.
- **Temporal subtraction** can give some indication in regard to the direction of movement of the cardiac boundaries. Again, this does not utilize prior knowledge about the global dynamics of the heart and may be overly sensitive to noise and artifacts. Some optical flow approaches may eliminate these limitations and were investigated in [39].
- **Temporal Smoothing** performs the segmentation of the 3-D volumes in parallel, while forcing the boundaries to move in a physically consistent way using temporal smoothing. In its simplest form, temporal smoothing could be achieved using an averaging function, $\Gamma_t = \Gamma_{(t-1)} + \Gamma_{(t+1)}/2\Delta t$, where Γ_t represents the boundary curve at time t .
- **Temporal consistency** of intensity values across the left ventricle cavity and the left ventricle myocardium was employed by Paragios and Deriche [40]. Similar to the previous approaches, artifacts present in the left ventricle cavity, due to the dynamics of blood during the cardiac cycle, may restrict the application of this method. Also, this method places confidence in the initial contextual values obtained from a statistical classifier that estimates tissue membership as a mixture of Gaussian distributions.
- **Database of Prior Image Models** created from a selection of images at particular temporal instances may be registered to the unseen image. Like other *a priori* models, this

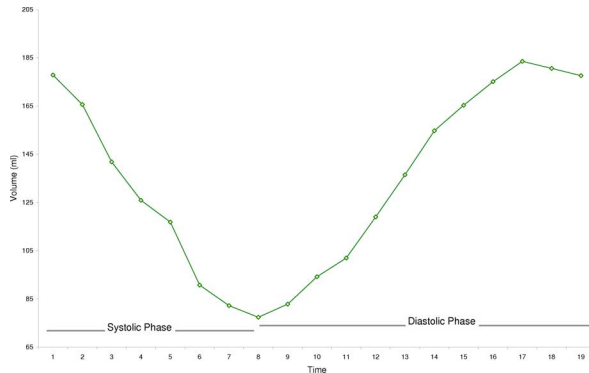


Fig. 1. Volume, in milliliters, of the left ventricle cavity over the cardiac cycle obtained from manually delineated cardiac boundaries.

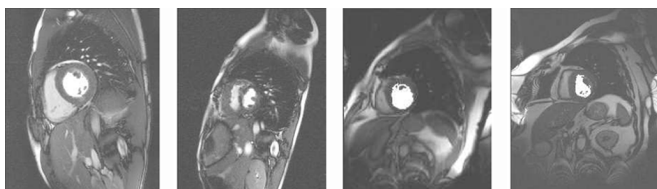


Fig. 2. Results show the initialization (marked in white) from a seeded Fast Marching algorithm. Method was applied to perform a robust initial estimate of the left ventricle cavity of the heart on four separate datasets displaying a high variability of the left ventricle shape. Images are courtesy of Dr. D. Pennell and Dr. J. Murray.

approach relies on building generic models that are applicable to a wide range of heart morphologies. Variations in cardiac morphology caused by individual anatomical features or disease may not be accounted for in such models.

- **Prior Temporal Parameterised Model** proposes to model the dynamics of the cardiac cycle and further refine this model as the parallel segmentation is performed on 3-D volumes. Unlike database models constructed in the image space, broader classification of the cardiac boundary’s movement during the entire cycle can be applied to all variations of heart morphologies. Exploiting the construct of the level-set function, the parameterized model can be determined and incorporated into the level-set update.

In our proposed algorithm, the segmentation of the 4-D MRI data is approached in a parallel sense using temporal constraints in an effort to control the boundary deformation away from erroneous spilling or over segmentation. The control of the boundary evolution is achieved by means of prior knowledge about the deformation of the cardiac muscle throughout a complete cardiac cycle. The general case for the data we have studied experimentally illustrates that the blood volume of the left ventricle follows a cyclical filling and emptying process similar to that illustrated in Fig. 1, which shows an example of a real patient data where the left ventricle is manually delineated in the short-axis stack. This temporal model can also be seen in Perperidis *et al.* [37] where it has been enforced during the segmentation process. The volume change over time is intrinsically linked to the boundary motion. In our method, we attempt to employ this intrinsic information to generate an initial weak model of boundary motion, which can evolve to

real data while providing supervision to the evolution of the boundary surfaces.

A. Modelling the Temporal Movement

Exploiting the formalization of the level-set function, the cardiac cycle as represented in Fig. 1 can be modelled for each 3-D point over time. Essentially, for each 3-D point in space, the distance to the contour represents the cardiac boundary increases and decreases. There is an associated constant (A) which defines a point’s initial distance to the contour. We model this movement of the contour using an inverted Gaussian function. A Gaussian function was shown to produce very good results experimentally. It can be computed quickly as it has a low number of parameters and it introduces a temporal smoothing over the cardiac cycle.

For the general Gaussian function defined in (7), the parameters A , B , μ , and σ can be found by fitting a Gaussian curve to each voxel within the narrow band over the cardiac cycle. Initial values are obtained from the Fast Marching algorithm. Gaussian model fitting is achieved using least squares approximation. In our experiments nonlinear fitting proved to be unstable due to the low number of volumes in the temporal resolution (~ 25). Therefore, linear least squares fitting was applied iteratively to a linearized form of the function until convergence was achieved. However, it is also possible to linearize a nonlinear function at the outset and still use linear methods for determining the fit parameters without resorting to iterative procedures. Equation (7) represents the equation that is fitted to each position of the function ϕ over the cardiac cycle

$$y(t) = A + Be^{-(t-\mu)^2/2\sigma^2}. \quad (7)$$

This fitted Gaussian represents the model for the dynamics of the cardiac muscle over the cardiac cycle. The deformation of the boundary surface of the level-set is constrained by this Gaussian model. In this way, the evolution of the level-set boundary can be constrained to contract and expand under Gaussian motion, where the saddle point is the temporal position given by μ and deformation occurs at a rate of σ . As each point on the function ϕ is defined as the distance to the zero level-set boundary, the Gaussian model can be fitted to each point within the narrowband.

The methodology is illustrated in Fig. 3, where a single point is selected within the narrowband. In Fig. 3, the boundary contracts and then expands in similar manner as the left ventricle boundary evolves from end-diastole to end-systole and back again to end-diastole. As this evolution takes place, the value at the point’s position grows and shrinks as the distance to the boundary increases and decreases. This evolution can be modelled using (7) where the parameters B , μ and σ are determined from the Fast Marching initialization. The value of A represents the offset of the Gaussian model. Fig. 4 illustrates the model applied to the long axis view.

B. Level-Set Influenced by an Adaptive Variance Gaussian

In order to use this information in the level-set evolution, an adaptive Gaussian model is developed. Similar to the general Gaussian model given in (7), the aim is to improve the models fit on the data. This results in the deformation of the boundary

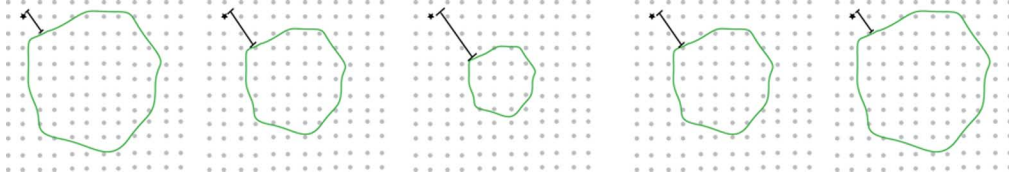


Fig. 3. Change of a single point on ϕ as the boundary evolves over the cardiac cycle in the short axis view.

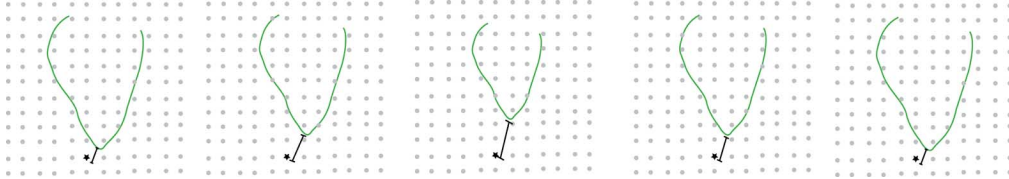


Fig. 4. Change of a single point on ϕ as the boundary evolves over the cardiac cycle in the long axis view.

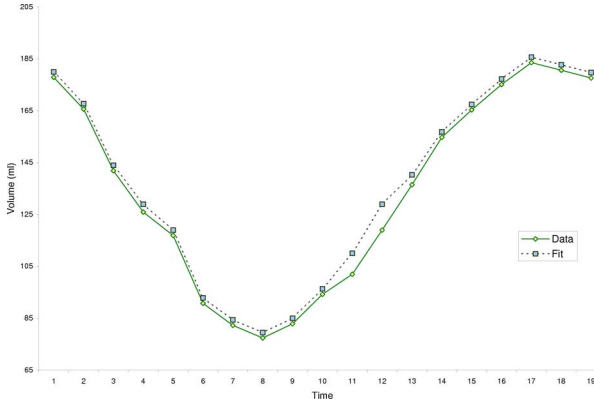


Fig. 5. Volume, in milliliters, of the left ventricle cavity over the cardiac cycle with fitted model using an adaptive Gaussian model.

where the temporal dynamics of the initial segmentation that are obtained using the Fast Marching algorithm are closely maintained during the boundary evolution process. In practice, this model is created by a least squares fitting of a Gaussian model where the variance (σ) is calculated separately at each temporal position. In essence this means that the least squares error is close to zero at each temporal position. This is illustrated in Fig. 5 where the model curve closely resembles the real data.

The incorporation of this new force into the level-set evolution is achieved as follows:

$$\frac{\partial \phi}{\partial t} = g(|\nabla I|)(c + \epsilon \kappa + \mathbf{K})|\nabla \phi| + \beta(\nabla I \cdot \nabla \phi) \quad (8)$$

where \mathbf{K} represents the normalized difference between the expected value, using the model described previously, and the actual value determined using the value of ϕ at each point within the narrowband. $g(|\nabla I|)$ represents the gradient information from the data, c is an advection force to grow the contour (in our implementation $c = 1$), and κ is the curvature term. ϵ and β are user defined control terms and were determined experimentally to be 0.025 and 0.05, respectively.

However, the temporal model created from the initialization may not represent the final segmentation of the target object, as too much confidence is placed on the initial model created

using the Fast Marching approach. For example, if the Fast Marching algorithm fails at one particular time sequence, the temporal model may incorporate this error. Using the curvature constraint, the level-set algorithm can overcome this error. Also, the temporal model that is created may not allow the level-set to deform greatly from the model created from the initialization. Therefore, a new approach is proposed that uses the information obtained from the initialization step but iteratively updates this model based on the evolution of the level-set at each iteration. This creates a smoothing effect on the level-set surfaces over the cardiac cycle but can also cope with poor initialization.

C. Level-Set Influenced Using EM

In order to address the limitations associated with the adaptive variance model described in the previous section, a novel approach is introduced which iteratively updates the initial parameters of the model. This essentially acts as a form of EM algorithm. The EM algorithm is a two step approach which aims to fit a model to data and is particularly useful where there is unknown or incomplete data. In the case of cardiac boundary segmentation, the observed data is defined as the value of the level-set function ϕ at a particular position over the entire cardiac cycle. The unknown or missing data is a final Gaussian model which is inferred on the deformation over the cardiac cycle. The EM algorithm takes initial parameters from the temporal model constructed using the Fast Marching algorithm. The Gaussian mixture model contains a single Gaussian function. In our experiments, it was found that a single Gaussian was deemed sufficient to handle the slight asymmetry of the cardiac cycle. More Gaussians could be added but as the temporal model is used as a loose model of dynamics, the extra computational expense of generating a close approximation to the initial data is not justified. Following the initialization, the algorithm performs an expectation or fit of the data at a particular temporal position to the overall temporal model, see Fig. 6. The results from this expectation stage are the differences between the model and the observed data. The expectation step which is given in (11) calculates the expected log-likelihood function for the complete temporal data using the estimates for the parameters of the temporal model defined in (7). The classic implementation of the

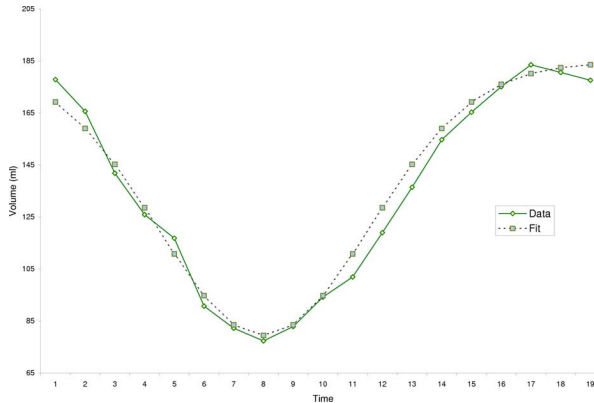


Fig. 6. Volume, in milliliters, of the left-ventricle cavity over the cardiac cycle with fitted model using an inverted Gaussian Model.

EM algorithm can work on a mixture of models, but in our case it is using just one model defined in (7) (see appendix for additional details on the EM algorithm).

The maximization step in this case is performed by deforming the level-set function ϕ based on the results from the expectation stage. Hence, the maximization step is defined by the update of (8) that is controlled by the parameter \mathbf{K} . From this expectation calculation, a maximization is performed to correct for the calculated differences. The process is iterative and the parameters for the model are reevaluated at each iteration.

This approach addresses the problems associated with the previous method. The results from the Fast Marching algorithm are used only as initial values for the EM algorithm. However, these initial parameters are reevaluated at each iteration, so errors from the Fast Marching approach are redressed during the evolution of the level-set algorithm.

IV. RESULTS

In order to assess the validity of this approach, the results of the segmentation using the iteratively optimized algorithm are compared against those obtained from expertly assisted segmentations of the left ventricle. The algorithm is applied to six unseen datasets from four different institutions with a high variation between datasets. The manual annotations were validated by an experienced cardiologist. Fig. 8 displays a linear plot and a Bland-Altman plot for the areas in 2-D of the manually traced boundaries. The error is calculated on the 2-D slices as manual segmentation was performed by tracing 2-D curves on the data slices. Therefore, all measurements are in mm^2 .

Point-to-curve errors for the adaptive variance approach and from the EM algorithm are shown in Table I. The results of the differences in area between the proposed algorithm and manual segmentation are displayed in Fig. 8, showing the linear regression plot and the Bland-Altman plot [41]. When the linear plot of the blood pool areas was compared against manual segmentation, the Gaussian curve method with adaptive variance produced a regression value of 0.71 while the optimised EM approach yielded a regression of 0.76. The Bland-Altman plot indicates good reproducibility of results. Compared to the work of Lorenzo-Valdés *et al.* [17], they report a regression value of 0.95 when evaluating the volume differences between their method and manual tracings. The main advantage of our method

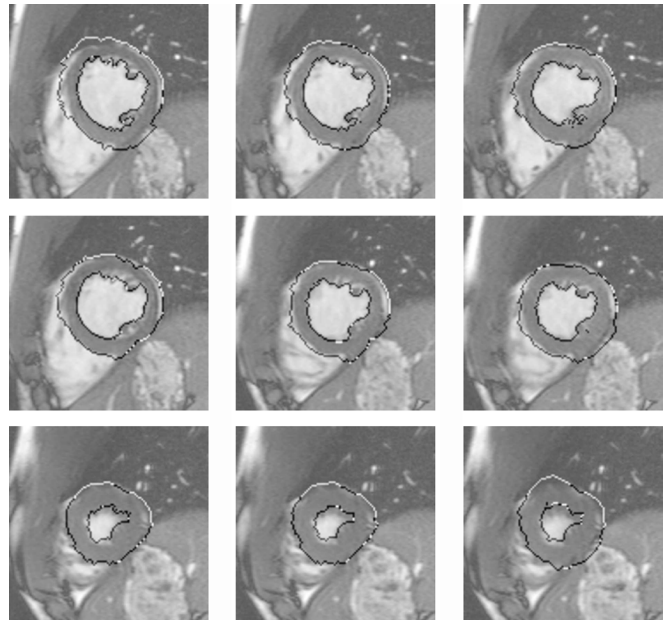


Fig. 7. Results from a coupled 4-D segmentation of a cardiac sequence for diastolic, systolic, and midphase for a basal (top row), midslice (middle row), and apical slice (bottom row).

over that presented by Lorenzo-Valdés *et al.* is that we do not model the data in the image space. We create a generic temporal model to loosely fit the data, assuming the sequence is captured over the entire heartbeat. Lorenzo-Valdés *et al.* use presegmented datasets that are temporally resampled to fit the number of sequences in the new data. Thus, they are bounded by the differences of the unseen data from their training data. While accurate in an assessment of volume data in a leave-one-out scenario, we believe that our method is more generic. Fritscher *et al.* [29] measure the similarity between manual and automatic segmentation based on overlap. The evaluation is performed on two datasets. Rueckert and Burger [42] report a 5% difference between their technique and the radiologists annotation.

Measuring overlap is achieved using Dice metric [43]. A_{ae}^k denotes the area of the pixels that are assigned to a class k by both the ground truth and the automatic algorithm. Similarly, A_a^k and A_e^k denote the areas of the pixels assigned to the segmented blood-pool by the automatic algorithm and the ground truth, respectively. The overlap between the automatic segmentation and the ground truth for class k is measured by $2A_{ae}^k / (A_a^k + A_e^k)$. Using this method, our algorithm returns a Dice metric of 0.81 ± 0.16 for all data analyzed. However, this metric can be influenced by the smaller areas around the apex where the difference in area is significantly higher when comparing to the area segmented.

Another advantage of our iteratively optimized algorithm, is that it guarantees convergence [44]–[46] and also reduces the error between the observed data and the model at each iteration. This means that convergence is faster than using the static model. This is characterized in Fig. 9 by measuring the error decay between the two methods based on synthetically generated phantom data.

The receiver operating characteristic (ROC) curves are displayed in Fig. 10 illustrating that the method using the EM approach achieves higher sensitivity and specificity than the adap-

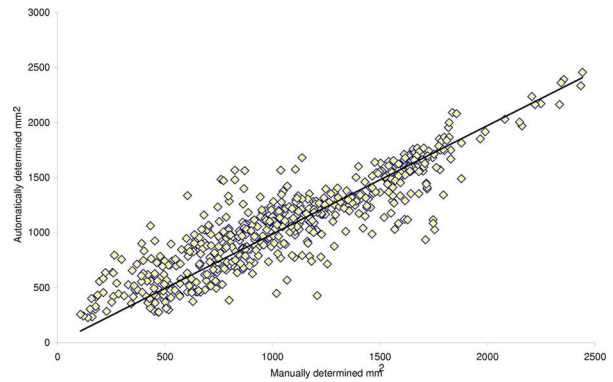
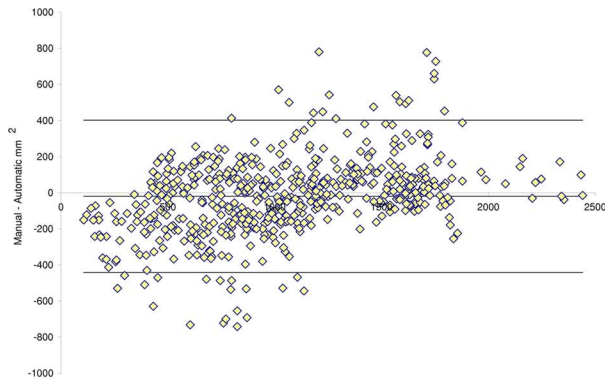


Fig. 8. Results of the 4-D segmentation of the left ventricle cavity boundary compared against those obtained from manual segmentation. Error analysis is performed on the 2-D slices and the results are presented in mm^2 .

TABLE I
POINT TO CURVE ERRORS FOR METHOD 1 USING THE GAUSSIAN CURVE WITH ADAPTIVE VARIANCE AND METHOD 2 USING THE EXPECTATION-MAXIMIZATION OF THE GAUSSIAN PARAMETERS. ALL MEASUREMENTS ARE IN MILLIMETERS

	Endo-cardial		
	Average	Std. Dev.	RMS
Method 1	2.4374	2.3168	3.3974
Method 2	1.2475	1.3369	1.8670

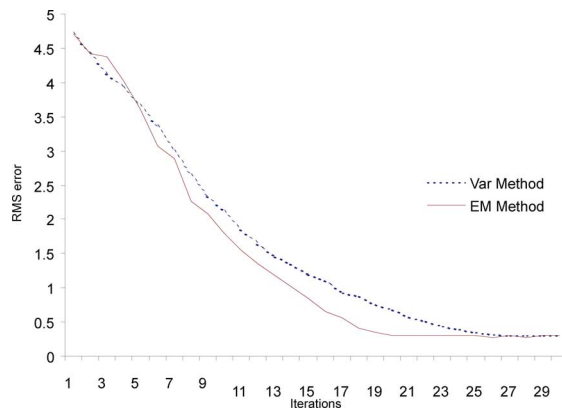


Fig. 9. Results show the error decay for both methods based on the 4-D segmentation of synthetically generated phantom data. RMS error is measured in pixels.

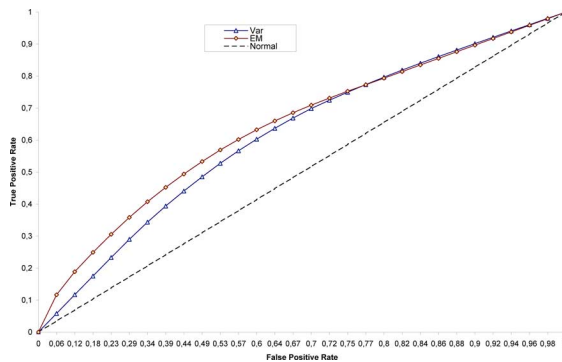


Fig. 10. ROC representing the sensitivity and specificity of the adaptive variance (Var) and using the EM methods over the deformation of the level-set on phantom data.

tive variance approach. The areas under the ROC curves are calculated to be 0.613 for the variance method and 0.636 for the EM

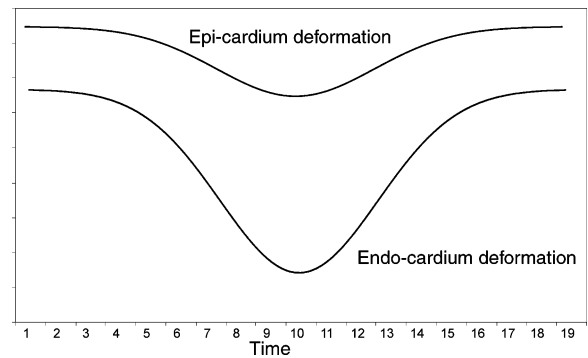


Fig. 11. Estimation using prior knowledge of the endo- and epi-cardial deformation throughout the cardiac cycle using inverse Gaussian curves.

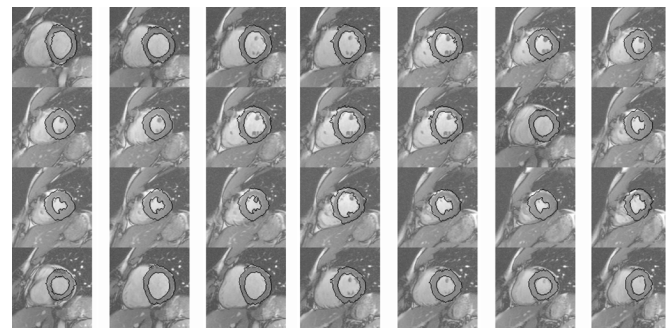


Fig. 12. Results from a coupled 4-D segmentation of a cardiac sequence.

method. The level-set approach is a surface growing algorithm and the slopes of the ROC curves are not as significant as those published for other classification methods.

A. Coupled Approach

Coupling of two level-sets can also be achieved in a coherent and intuitive way by using two Gaussian models, as illustrated in Fig. 11. The outer contour represents the epi-cardial boundary and is initialized a distance of five pixels from the Fast Marching result. Similarly, at each point on the grid, the parameters for the two Gaussian models representing the evolution of the endo- and epi-cardial boundaries are stored. After optimization, the evolution of the epi-cardial boundary is less pronounced and the Gaussian model is shallower. Results from a coupled segmentation are illustrated in Figs. 7 and 12 for different time phases and slice locations.

V. CONCLUSION

In this paper, deformable contours for feature extraction in medical imaging were introduced and discussed. An overview of the current state-of-the-art methods used for the segmentation of the left ventricle of the heart was given.

In the following sections, a new general solution to left ventricle segmentation from 4-D MRI data was presented. Modelling cardiac muscle motion over the cardiac cycle was employed to loosely guide a contour growing algorithm. Information obtained from a Fast Marching segmentation was used to set the initial values in a parametric model describing the cardiac motion. The model is based on nonrigid deformation of the left ventricle boundaries over time using prior knowledge about cardiac dynamics. After each evolution of the level-set algorithm, the model is optimized to the data using an EM algorithm to reduce the target to object errors.

The developed segmentation algorithm produces accurate results when compared to expertly assisted segmentations of the left ventricle boundaries. The algorithm was tested on data containing high variation, both in anatomical morphology and acquisition parameters. Finally, the results are illustrated for a coupled surface segmentation where the left ventricle inner and outer boundaries are tracked in a computationally efficient way using two separate models of temporal motion.

APPENDIX

The EM algorithm satisfies the necessity in our approach to estimate the parameters of a probability distribution function. In our case, we are looking to estimate the mean and standard deviation of myocardial deformation throughout the cardiac cycle.

The approach consists of two steps, the expectation (E) step and a maximization (M) step. Consider the general case of a d -dimensional random variable $x = [x_1, x_2, x_3, \dots, x_d]^T$ and suppose it follows a k -component finite mixture distribution. We assume it follows a mixture of Gaussian curves. Initial values for the Gaussian's mean and variance are estimated using the variance of the data. Its' probability density function (pdf) could be written as

$$p(x|\theta) = \sum_{m=1}^k \alpha_m p(x|\theta_m) \quad (9)$$

where α_m is the mixing parameter for each of the Gaussian mixture models (GMM) and $\theta_m = \{\mu_m, \sigma_m\}$ are the Gaussian's parameters

$$\alpha_m \geq 0, \text{ and } \sum_{m=1}^k \alpha = 1. \quad (10)$$

The algorithm is built on an iterative scheme and consists of two steps. The first, the E -step, calculates the expected log-likelihood function for the complete data that is defined by Q using the estimates for the parameters $\hat{\theta}(t)$

$$Q(\theta, \hat{\theta}(t)) \equiv E[\log p(X, Y|\theta)|X, \hat{\theta}(t)]. \quad (11)$$

The second, M -step, uses the maximized values of this result to generate the next set of parameters

$$\hat{\theta}(t+1) = \arg \max_{\theta} Q(\theta, \hat{\theta}(t)). \quad (12)$$

The algorithm iterates between (11) and (12) until convergence is reached. It is important to note that local convergence of the EM algorithm is assured [44]–[46]. In our case, k is set to one as there is just one underlying motion that concerns us. This reduces the effects of binning and dropouts to a certain extent as a single Gaussian is calculated over the full cardiac cycle.

ACKNOWLEDGMENT

The cardiac studies used in this paper were kindly donated by Dr. J. Murray and staff of the Mater Misericordiae Hospital, Dublin, Ireland, Dr. R. van der Geest of Leiden University, Holland, with permission from Cory Swingen, University of Minnesota, Minneapolis, Dr. D. Rueckert, Imperial College London, and Dr. D. Pennell and staff of Imperial College Hospital London, U.K. The authors would also like to thank Dr. J. Murray for his advice and validation of segmented data and for assessing the value of this work from a medical point of view. M. Lynch performed this work while with the Vision Systems Group in Dublin City University

REFERENCES

- [1] A. Rodgers and P. Vaughan, *The World Health Report 2002*. Geneva, Switzerland: The World Health Organisation, 2002.
- [2] S. Petersen, V. Peto, M. Rayner, J. Leal, R. Luengo-Fernandez, and A. Gray, *European cardiovascular disease statistics* British Heart Foundation, London, U.K., 2005.
- [3] A. F. Frangi, W. J. Niessen, and M. A. Viergever, "Three-dimensional modelling for functional analysis of cardiac images: A review," *IEEE Trans. Med. Imag.*, vol. 20, no. 1, pp. 2–25, Jan. 2001.
- [4] J. S. Suri, S. K. Setarehdan, and S. E. Singh, *Advanced Algorithmic Approaches to Medical Image Segmentation: State-Of-The-Art Applications In Cardiology, Neurology, Mammography and Pathology*. Berlin: Springer, 2002.
- [5] M. Kass, A. Witkin, and D. Terzopoulos, "Snakes: Active contour models," in *Int. J. Comput. Vis.*, 1988, vol. 1, pp. 321–331.
- [6] L. H. Staib and J. S. Duncan, "Boundary finding with parametrically deformable models," *IEEE Trans. Pattern Anal. Mach. Intell.*, vol. 14, no. 11, pp. 1061–1075, Nov. 1992.
- [7] L. Staib and J. Duncan, "Model-based deformable surface finding for medical images," *IEEE Trans. Med Imag.*, vol. 15, no. 5, pp. 720–731, Oct. 1996.
- [8] H. Delingette, M. Hébert, and K. Ikeuchi, "Shape representation and image segmentation using deformable surfaces," *Image and Vision Comput.*, vol. 10, no. 3, pp. 132–144, Apr. 1993.
- [9] L. D. Cohen, "On active contour models and balloons," *CVGIP: Image Understand.*, vol. 53, pp. 211–218, 1991.
- [10] M. Sermesant, C. Forest, X. Pennec, H. Delingette, and N. Ayache, "Deformable biomechanical models: Application to 4-D cardiac image analysis," *Med. Image Anal.*, vol. 7, no. 4, pp. 475–488, 2003.
- [11] D. Molloy and P. W. Whelan, "Active-meshes," *Pattern Recogn. Lett.*, vol. 21, pp. 1071–1080, 2000.
- [12] T. Cootes, C. Taylor, A. Hill, and J. Halsm, "The use of active shape model for locating structures in the medical image," *Image Vis. Comput.*, vol. 12, no. 6, pp. 355–366, 1994.
- [13] T. F. Cootes, G. J. Edwards, and C. J. Taylor, "Active appearance models," *Lecture Notes Comput. Sci.*, vol. 1407, pp. 484–498, 1998.
- [14] M. B. Stegmann, H. Ólafsdóttir, and H. B. W. Larsson, "Unsupervised motion-compensation of multi-slice cardiac perfusion MRI," *Med. Image Anal.*, vol. 9, no. 4, pp. 394–410, 2005.

- [15] B. P. F. Lelieveldt, S. C. Mitchell, J. G. Bosch, R. J. van der Geest, M. Sonka, and J. H. C. Reiber, "Quantification of cardiac ventricular function using magnetic resonance imaging (MRI) and multi slice computed tomography (MSCT)," in *Proc. Inf. Process. Med. Imag.*, Davis, CA, , 2001, vol. 18-22fs, pp. 446–452.
- [16] S. C. Mitchell, B. P. F. Lelieveldt, J. G. Bosch, R. Van der Geest, J. H. C. Reiber, and M. Sonka, "Segmentation of cardiac MR volume data using 3-D active appearance models," in *Proc. SPIE Int. Soc. Eng.*, 2002, vol. 4684 I, pp. 433–443.
- [17] M. Lorenzo-Vald´s, G. I. Sanchez-Ortiz, A. G. Elkington, R. H. Mohiaddin, and D. Rueckert, "Segmentation of 4-D cardiac MR images using a probabilistic atlas and the EM algorithm," *Med. Image Anal.*, vol. 8, pp. 255–265, 2004.
- [18] S. Osher and J. A. Sethian, "Fronts propagating with curvature dependent speed: Algorithms based on hamilton-jacobi formulations," *J. Comput. Phys.*, pp. 12–49, 1988.
- [19] R. Malladi, J. A. Sethian, and B. C. Vemuri, "Shape modeling with front propagation: A level set approach," *IEEE Trans. Pattern Anal. Mach. Intell.*, vol. 17, no. 2, pp. 158–175, Feb. 1995.
- [20] R. Malladi and J. A. Sethian, "Level set methods for curvature flow, image enhancement, and shape recovery in medical images," in *Proc. Conf. Visualization Math.*, Berlin, Germany, Jun. 1997.
- [21] V. Caselles, F. Catté, T. Coll, and F. Dibos, "A geometric model for active contours in image processing," *Numer Math*, vol. 66, no. 1, pp. 1–31, Dec. 1993.
- [22] V. Caselles, R. Kimmel, and G. Sapiro, "Geodesic active contours," *Int. J. Comp. Vision*, vol. 22, no. 1, pp. 61–79, 1997.
- [23] W. J. Niessen, B. M. ter Haar Romeny, and M. A. Viergever, "Geodesic deformable models for medical image analysis," *IEEE Trans. Med. Imag.*, vol. 17, no. 4, pp. 634–642, Aug. 1998.
- [24] J. Suri, K. Liu, S. Singh, S. Laxminarayana, and L. Reden, "Shape recovery algorithms using level sets in 2-D/3-D medical imagery: A state-of-the-art review," *IEEE Trans. Inf. Technol. Biomed.*, vol. 6, no. 1, pp. 8–28, Mar. 2002.
- [25] E. D. Angelini, Y. Jin, and A. F. Laine, "Handbook of medical image analysis: Advanced segmenation and registration models," in *State-of-the-Art of Levelset Methods in Segmentation and Registration of Medical Imaging Modalities*. Norwell, MA: Kluwer, 2004.
- [26] V. Caselles, R. Kimmel, and G. Sapiro, "Geodesic active contours," in *Proc. 5th Int. Conf. Comput. Vision*, Jun. 1995, pp. 694–699.
- [27] J. A. Sethian, "A marching level set method for monotonically advancing fronts," in *Proc. Natl. Acad. Sci.*, 1996, vol. 93, pp. 1591–1595.
- [28] D. Adalsteinsson and J. A. Sethian, "A fast level set method for propagating interfaces," *J. Comput. Phys.*, vol. 118, no. 2, pp. 269–277, May 1995.
- [29] K. D. Fritscher, R. Pilgram, and R. Schubert, "Automatic cardiac 4-D segmentation using level sets," in *Proc. of Functional Imaging and Modelling of the Heart*, A. Frangi, Ed. : Springer, 2005, Lecture Notes in Computer Science, pp. 113–122.
- [30] E. Bardinet, L. Cohen, and N. Ayache, "Tracking and motion analysis of the left ventricle with deformable superquadratics," *Med. Image Anal.*, vol. 1, no. 2, pp. 129–149, 1996.
- [31] T. McInerney and D. Terzopoulos, "A dynamic finite element surface model for segmentation and tracking in multidimensional medical images with application to 4-D image analysis," *Comput. Med. Imag. Graph.*, vol. 19, no. 1, pp. 69–83, Jan. 1995.
- [32] D. Rueckert and P. Burger, "Shape-based segmentation and tracking in 4-D cardiac MR images," in *Proc. Int. Conf. Computer Vision, Virtual Reality Robotics Medicine, CVRMed.*, Grenoble, France, 1997, pp. 43–52.
- [33] W. Sun, M. Çetin, R. Chan, V. Reddy, G. Holmvang, V. Chandar, and A. S. Willsky, "Segmenting and tracking the left ventricle by learning the dynamics in cardiac images," *Inf. Process. Med. Imag. (IPMI)*, pp. 553–565, 2005.
- [34] J. C. McEachen, II and J. S. Duncan, "Shape-based tracking of left ventricular wall motion," *IEEE Trans. Med. Imag.*, vol. 16, no. 3, pp. 270–283, Mar. 1997.
- [35] N. Paragios, "A variational approach for the segmentation of the left ventricle," *Int. J. Comput. Vis.*, pp. 345–362, 2002.
- [36] ———, "4-D deformable models with temporal constraints: Application to 4-D cardiac image segmentation," *Med. Image Anal.*, vol. 9, no. 1, pp. 87–100, Feb. 2005.
- [37] D. Perperidis, A. Rao, M. Lorenzo-Valdés, R. Mohiaddin, and D. Rueckert, "Spatio-temporal alignment of 4-D cardiac MR images," in *Functional Imaging and Modeling of the Heart*. New York: Springer-Verlag, 2003, pp. 205–214.
- [38] D. Perperidis, R. Mohiaddin, and D. Rueckert, "Spatio-temporal free-form registration of cardiac MR image sequences," in *Medical Image Computing and Computer-Assisted Intervention–MICCAI*. Berlin, , Germany: Springer, 2004, pp. 911–919.
- [39] J. L. Barron, "Experience with 3-D optical flow on gated MRI cardiac datasets," in *Proc. 1st Canadian Conf. Comput. Robot Vision*, May 2004, pp. 370–377.
- [40] N. Paragios and R. Deriche, "Geodesic active regions: A new paradigm to deal with frame partition problems in computer vision," *J. Vis. Comm. Image Rep.*, vol. 13, no. 2, pp. 249–268, 2002.
- [41] J. M. Bland and D. G. Altman, "Statistical methods for assessing agreement between 2 methods of clinical measurement," *Lancet*, vol. 8476, pp. 307–310, 1986.
- [42] D. Rueckert, P. Burger, S. M. Forbat, R. Mohiaddin, and G. Z. Yang, "Automatic tracking of the aorta in cardiovascular MR images using deformable models," *IEEE Trans. Med. Imag.*, vol. 16, no. 5, pp. 581–590, Oct. 1997.
- [43] L. R. Dice, "Measures of the amount of ecologic association between species," *Ecology*, vol. 26, no. 3, pp. 297–302, 1945.
- [44] L. Xu, "On convergence properties of the EM algorithm for gaussian mixtures," *Neural Comput.*, vol. 8, no. 1, pp. 129–151, Jan. 1996.
- [45] A. Dempster, N. Laird, and D. Rubin, "Maximum likelihood from incomplete data via the EM algorithm," *J. Roy. Statist., Ser. B*, vol. 39, no. 1, pp. 1–38, 1977.
- [46] J. Bilmes, A gentle tutorial of the EM algorithm and its application to parameter estimation for gaussian mixture and hidden markov models Univ. Berkeley, Berkeley, CA, Tech. Rep. TR-97-021, 1998.